Contribution from the Department of Chemistry,
The University of Houston, Houston, Texas 77004

Dirhodium Complexes with Axially and Equatorially Nonequivalent Rhodium Atoms. Characterization of $Rh_2(tcl)_4(tclH)$ and $Rh_2(tcl)_4(CO)$ (tcl = ω-Thiocaprolactamate)

R. S. Lifsey, M. Y. Chavan, L. K. Chau, M. Q. Ahsan, K. M. Kadish,* and J. L. Bear*

Received August 14, 1986

The reaction of $Rh_2(O_2CCH_3)_4$ with ω-thiocaprolactam gives a polar dirhodium(II) complex with four bridging ω-thiocaprolactamate (tcl) ions and one axially bound ω-thiocaprolactam ligand. The structure of $Rh_2(tcl)_4(tclH)$ and the carbon monoxide adduct $Rh_2(tcl)_4(CO)$ have been determined by X-ray crystallography. $Rh_2(tcl)_4(tclH)$ (**1**) crystallizes in the space group $P2_1/n$ (monoclinic) with lattice constants of a = 11.762 (2) Å, b = 22.092 (6) Å, c = 14.533 (4) Å, β = 104.56 (2)°, and V = 3656 Å^3. The structure analysis converged to R = 0.019 and R_w = 0.022. $Rh_2(tcl)_4(CO)$ (**2**) crystallizes in the space group $P4nc$ (tetragonal) with cell constants of a = 11.418 (2) Å, c = 11.410 (2) Å, and V = 1488 Å^3 with R = 0.022 and R_w = 0.031. The prominent feature common to compounds **1** and **2** is the arrangement of the bridging ions such that all four sulfur atoms are bound to one rhodium, Rh1, and an average Rh–S bond distance of 2.354 Å. The axial Rh–S bond distance of 2.388 Å is relatively short compared to other Rh–S axial bond distances. The second rhodium, Rh2, is bound equatorially to four nitrogens with an average Rh–N bond distance of 2.025 Å. The axial position of Rh2 is vacant. A long Rh–Rh bond distance of 2.497 (1) Å was found. Compound **2** has the same basic structure as compound **1** except that CO occupies the axial position at Rh1 instead of tclH. The Rh–C distance of 1.913 Å for the rhodium–carbonyl bond falls within the range of other rhodium complexes with terminal carbonyls. A nonequivalence of the rhodium centers is not evident from the ESR spectrum of $[Rh_2(tcl)_4]^+$ since the species does not show resolved hyperfine splitting in $g_\parallel$. Half-wave potentials for oxidation of the three complexes increase in the order $Rh_2(tcl)_4 < Rh_2(tcl)_4(tclH) < Rh_2(tcl)_4(CO)$. This indicates a lowering of the HOMO upon tclH or CO binding. The lowering of the HOMO due to CO binding is extremely large (0.45 V). The axial tclH ligand of compound **1** is kinetically inert to substitution by other ligands such as pyridine and phosphines. This is unlike the case for other dirhodium(II) complexes, which are axially labile. The substitution of CO for tclH is also relatively slow, and kinetic data show that the substitution of tclH by CO is first order in $Rh_2(tcl)_4(tclH)$ and CO. A mechanism for the exchange process is discussed.

Introduction

The synthesis and crystal structure of a dirhodium complex with a polar Rh–Rh bond, dirhodium(II) tetrakis(6-fluoro-2-oxypyridinate), $Rh_2(fhp)_4$, has recently been reported.[1] One rhodium is bonded only to nitrogen atoms of the four fhp bridging ligands, and the other rhodium is bonded only to oxygen atoms of the same ligands. The reason for the formation of the polar complex has been proposed to be steric in nature. However, it is not clear how such complexes with polar Rh–Rh bonds differ from those with nonpolar Rh–Rh bonds in terms of their various chemical and physical properties.

A number of dirhodium(II) complexes of the type $Rh_2(RNOCR')_4$ have been reported with R = H, Ph and R' = H, CH_3, CF_3.[3-9] Although a distribution of four nitrogen donor atoms around one Rh atom in $Rh_2(fhp)_4$ is conceivable, this 4,0 isomer is not formed in any of the $Rh_2(RNOCR')_4$ complexes. $Rh_2(HNOCCH_3)_4$ forms a single 2,2 cis complex with the four nitrogen and four oxygen donor atoms equally distributed around the two rhodium atoms.[12,13] $Rh_2(PhNOCCH_3)_4$ forms two isomers, one of which has a 2,2 cis configuration. The other isomer has a 3,1 distribution of the nitrogen donor atoms bound to the two rhodiums.[9] Dirhodium thioacetate, $Rh_2(SOCCH_3)_4$, has bridging ligands that contain mixed S and O donor atoms, and this complex also has only two sulfur and two oxygen atoms attached to each rhodium in a cis arrangement.[14] Dirhodium complexes with lactamate ligands, $Rh_2(lactam)_4$ (where lactam = valerolactamate, pyrrolidinonate), have also been synthesized[15] but no structure other than that of the 2,2 cis isomer described above has been obtained.

$Rh_2(O_2CCH_3)_n(RNOCR')_{4-n}$ complexes with n = 1 and n = 3 can be considered somewhat polar in consequence of the differences in the number of nitrogen atoms bonded to each rhodium. However, the ESR spectra of the corresponding singly oxidized $[Rh_2(O_2CCH_3)_n(RNOCR')_{4-n}(L)_2]^+$ complexes, where L is an axial ligand, suggests that the rhodium atoms are electronically equivalent, regardless of the value of n.[6,8,9] The two rhodium atoms in a given dirhodium complex can become electronically nonequivalent if their axial environments are different.[11]

In this paper we report the syntheses, crystal structures, electrochemistry, and ESR properties of the two dirhodium complexes $Rh_2(tcl)_4(tclH)$ and $Rh_2(tcl)_4(CO)$, with tcl = $^-\overline{NC(S)CH_2(CH_2)_3CH_2}$ (ω-thiocaprolactamate). In both, the Rh–Rh bonds are polar because of differences in the equatorial and axial environment of the two rhodium atoms. The properties of these complexes are then compared with those of so-called nonpolar dirhodium complexes reported in the literature.[2-13]

Experimental Section

Chemicals. $Rh_2(O_2CCH_3)_4$ was synthesized from $RhCl_3 \cdot 3H_2O$ (Alfa Inorganics) by a known procedure.[16] The ligand, ω-thiocaprolactam (tclH), was purchased from Aldrich Chemical Co. and was recrystallized from CH_2Cl_2 before use. Acetonitrile (CH_3CN) and 1,2-dichloroethane ($C_2H_4Cl_2$) (both of reagent grade) were dried by distillation over calcium hydride. The supporting electrolyte, tetrabutylammonium perchlorate (TBAP), was recrystallized from ethanol and vacuum-dried before use. Carbon monoxide and nitrogen were purchased from Matheson and Linde, respectively. The ^{13}C-labeled CO (99+%) was obtained from KOR Isotopes.

(1) Cotton, F. A.; Han, S.; Wang, W. *Inorg. Chem.* **1984**, *23*, 4762.
(2) Felthouse, T. R. *Prog. Inorg. Chem.* **1982**, *29*, 73.
(3) Dennis, A. M.; Howard, R. A.; Lancon, D.; Kadish, K. M.; Bear, J. L. *J. Chem. Soc., Chem. Commun.* **1982**, 339.
(4) Kadish, K. M.; Lancon, D.; Dennis, A. M.; Bear, J. L. *Inorg. Chem.* **1982**, *21*, 2987.
(5) Duncan, J.; Malinski, T.; Zhu, T. P.; Hu, Z. S.; Kadish, K. M.; Bear, J. L. *J. Am. Chem. Soc.* **1982**, *104*, 5507.
(6) Bear, J. L.; Zhu, T. P.; Malinski, T.; Dennis, A. M.; Kadish, K. M. *Inorg. Chem.* **1984**, *23*, 674.
(7) Zhu, T. P.; Ahsan, M. Q.; Malinski, T.; Kadish, K. M.; Bear, J. L. *Inorg. Chem.* **1984**, *23*, ?.
(8) Chavan, M. Y.; Zhu, T. P.; Lin, X. Q.; Ahsan, M. Q.; Bear, J. L.; Kadish, K. M. *Inorg. Chem.* **1984**, *23*, 4538.
(9) Lifsey, R. S.; Lin, X. Q.; Chavan, M. Y.; Ahsan, M. Q.; Kadish, K. M.; Bear, J. L. *Inorg. Chem.*, following paper in this issue.
(10) Cotton, F. A.; Felthouse, T. R. *Inorg. Chem.* **1981**, *20*, 584.
(11) Le, J. C.; Chavan, M. Y.; Chau, L. K.; Bear, J. L.; Kadish, K. M. *J. Am. Chem. Soc.* **1985**, *107*, 7195.
(12) Chavan, M. Y.; Lin, X. Q.; Ahsan, M. Q.; Bernal, I.; Bear, J. L.; Kadish, K. M. *Inorg. Chem.* **1986**, *25*, 1281.
(13) Ahsan, M. Q.; Bear, J. L.; Bernal, I. *Inorg. Chem.* **1986**, *25*, 260.
(14) Dikareva, L. M.; Sadikov, G. G.; Porai-Koshits, M. A.; Golubnichaya, M. A.; Baranovshii, I. B.; Shchelokov, R. N. *Russ. J. Inorg. Chem. (Engl. Transl.)* **1977**, *22*(7), 1093.
(15) Lifsey, R. S.; Ahsan, M. Q.; Chau, L. K.; Chavan, M. Y.; Kadish, K. M.; Bear, J. L., manuscript in preparation.
(16) Kitchens, J. F.; Bear, J. L. *J. Inorg. Nucl. Chem.* **1969**, *31*, 2415.

0020-1669/87/1326-0822$01.50/0

Table I. Data Collection and Processing Parameters

	$Rh_2(tcl)_4(tclH)$	$Rh_2(tcl)_4(CO)$
space group	$P2_1/n$, monoclinic	$P4nc$, tetragonal
cell constants		
a, Å	11.765 (2)	11.418 (2)
b, Å	22.092 (6)	
c, Å	14.533 (4)	11.410 (2)
β, deg	104.56 (2)	
V, Å^3	3656	1488
mol formula	$Rh_2S_5N_5C_{30}H_{51}$	$Rh_2S_4ON_4C_{25}H_{40}$
fw	847.9	746.74
formula units/cell (Z)	4	2
density (ρ), g cm^{-3}	1.54	1.67
abs coeff (μ), cm^{-1}	11.91	13.8
radiation (Mo Kα) (λ), Å	0.710 73	0.710 73
collection range, deg	$4 \le 2\theta \le 35$	$4 \le 2\theta \le 60$
scan width ($\Delta\omega$), deg	$0.90 \pm 0.35 \tan\theta$	$0.90 + 0.35 \tan\theta$
max scan time, s	150	120
scan speed range, deg min^{-1}	0.6–5.0	0.7–5.0
total data collected	2570	1312
indep data, $I > 3\sigma(I)$	2196	885
total variables	379	84
R^a	0.019	0.022
$R_w{}^a$	0.022	0.031

$^a R = \sum||F_o| - |F_c||/\sum|F_o|$ and $R_w = [\sum w(|F_o| - |F_c|)^2/\sum w|F_o|^2]^{1/2}$ with weights $w = \sigma_{F^2}$.

Synthesis of $Rh_2(tcl)_4(tclH)$. A mixture of ω-thiocaprolactam (2.3 g, 18 mmol) and $Rh_2(O_2CCH_3)_4$ (0.20 g, 0.45 mmol) was placed in an evacuated 25-mL round-bottom flask. The mixture was heated to a melt at 125 °C and magnetically stirred for 2–3 h. At this point the original green melt turned dark reddish brown and the reaction was stopped. The mixture was then dissolved in CH_2Cl_2. Upon evaporation, this solution gave large green-black crystals of $Rh_2(tcl)_4(tclH)$ (yield ~40%).

Synthesis of $Rh_2(tcl)_4(CO)$. This compound was synthesized by passing high-purity carbon monoxide gas through a solution of the $Rh_2(tcl)_4(tclH)$ in CH_2Cl_2 for 20–30 min. The solution color changed from green to red, and $Rh_2(tcl)_4(CO)$ precipitated either as an orange powder or as red crystals. The precipitate was filtered and collected, and the process was repeated until a complete exchange was achieved. The compound was purified by column chromatography with silica gel and CH_2Cl_2 as eluent. IR: $\bar{\nu}(CO)$ = 2025.4 cm^{-1} in $C_2H_4Cl_2$ and 2004.3 cm^{-1} in Nujol.

Instrumentation. An IBM Model 9400 UV–visible spectrophotometer was used for kinetic studies and a BAS-100 electrochemical analyzer for electrochemical studies. An arrangement of gas-flow controllers and a Matheson Model 8250 Dyna-blender were used to mix N_2 and CO in order to control the CO partial pressure. ESR spectra were recorded on an IBM Model ER 100 ESR spectrometer. The working electrode consisted of a platinum button, a platinum-wire auxiliary electrode, and a saturated calomel electrode (SCE) as a reference electrode. Nuclear magnetic resonance spectra were obtained with a Nicolet NT-300 WB spectrometer. A 12-mm broad-band probe tuned to 75.461 MHz was used for ^{13}C NMR acquisition. Infrared spectra were taken in solution with an IBM FT-IR/32 spectrometer.

Kinetic Studies of CO Binding. The kinetics of tclH substitution by CO was monitored in a visible spectroscopic cell, equipped with gas inlet. This was connected to Matheson Dyna-blenders and electronic gas-flow meters to control flow rates of CO and N_2 at the desired partial pressures of the components. The outlet was vented into an efficient exhaust hood. The inlet and outlet tubes were connected outside the cell, and close to it, in order to provide a valved alternate path (shunt) for the gas mixture. A desired gas mixture was bubbled through the solution for 60 s, after which the shunt was opened, thus stopping the solution purge but resulting in a constant composition of the gas above the solution throughout the experiment.

X-ray Data: $Rh_2(tcl)_4(tclH)$. A large reddish black prismatic block of dimensions 0.60 mm × 0.40 mm × 0.40 mm was mounted on a glass fiber in a random orientation on an Enraf-Nonius CAD-4 automatic diffractometer. The radiation used as Mo Kα monochromatized by a dense graphite crystal assumed for all purposes to be 50% imperfect. Final cell constants, as well as other information pertinent to data collection and refinement, are listed in Table I. The Laue symmetry was determined to be $2/m$, and from the systematic absences noted the space group was shown unambiguously to be $P2_1/n$. Intensities were measured by using the θ–2θ scan technique, with the scan rate depending on the net count obtained in rapid prescans of each reflection. Two standard reflections, monitored periodically during the course of the data collection as a check of crystal stability and electronic reliability, did not vary significantly. No correction for absorption was made due to the small absorption coefficient.

The structure was solved by MULTAN,[17] which revealed the positions of two Rh, five S, and two N atoms. The remaining non-hydrogen atoms were found in subsequent difference Fourier syntheses. The molecule was found to have a 4,0 arrangement of equatorial ligands, with a fifth thiocaprolactam ligand bound axially to the Rh atom with the four sulfurs. The usual sequence of isotropic and anisotropic refinement was followed, after which all hydrogens were entered in ideal calculated positions. The single exception was H5, which was located in a difference map and refined with a fixed thermal parameter. Hydrogen isotropic temperature factors were estimated on the basis of the thermal motion of the associated carbons. After all shift/esd ratios were less than 0.1, convergence was deemed reached at the agreement factors listed in Table I. No unusually high correlation coefficients were noted between any of the variables in the last cycle of least-squares refinement, and the final difference density map showed no peaks greater than 0.20 e/Å^3. All calculations were made with Molecular Structure Corp.'s TEXRAY 230 modifications of the SDP-PLUS series of programs.

$Rh_2(tcl)_4(CO)$. A large ruby red prismatic crystal (0.60 mm × 0.60 mm × 0.50 mm) was treated essentially as reported above. The details are listed in Table I. The lattice constants appear to be cubic. However, this is actually one of those exceedingly rare cases where the pattern of diffracted intensities does not support the apparent crystal symmetry on the basis of unit cell dimensions alone. The Laue symmetry was determined to be $4/mmm$, and from the noted systematic absences the space group was shown to be either $P4/mnc$ or $P4nc$. Since there are only two molecules in the unit cell, and since the molecule cannot have $4/m$ symmetry, space group $P4nc$ was assumed from the outset.

The structure was solved by simply placing one of the Rh atoms on the fourfold axis and identifying the remaining atoms in subsequent difference Fourier syntheses. The asymmetric unit comprises only one-fourth of a molecule, with the two Rh and axial carbonyl atoms all lying on the fourfold axis. The sense of direction in this polar, nonenantiomorphous space group was determined by analysis of 15 Bijvoet pairs of reflections[18] showing the greatest difference in F for the (+++) and (---) refinements. The difference between the R values of the two separate refinements was negligible.

Results and Discussion

Crystal and Molecular Structure of $Rh_2(tcl)_4(tclH)$. The most notable feature of the molecular structure (Figure 1) is that all four sulfur atoms are bound to the same rhodium (Rh1), which also is bound to the axial tclH ligand. The average Rh–S equatorial distance is 2.354 Å (Table III) based on Table II. The axial Rh–S bond distance, 2.388 Å, is relatively short compared to others (2.449–2.551 Å) that have been reported.[2,12] The second rhodium (Rh2) is bound equatorially to four nitrogens with ⟨Rh–N⟩ = 2.025 Å, and the axial position is vacant.

Substituting a sulfur donor for oxygen in the amide bridging ion considerably lengthens the Rh–Rh bond. For example, $Rh_2(tcl)_4(tclH)$ has one axial ligand and the Rh–Rh bond distance is 2.497 Å. The only known tetrabridged dirhodium(II) complex that has a longer Rh–Rh bond distance (2.550 Å) is $Rh_2(SOCCH_3)_4(HSOCCH_3)_2$.[14] It should be pointed out that this latter molecule has two sulfur and two oxygen donor atoms bound to each rhodium ion in a cis arrangement. There are also two long (2.521 Å) Rh–S axial bonds in this complex. The shorter Rh–S (axial) and Rh–Rh bond distances in $Rh_2(tcl)_4(tclH)$ compared to those in $Rh_2(SOCCH_3)_4(HSOCCH_3)_2$ are related to the former complex having only one axial ligand; at least the calorimetric data for the Me_2SO mono- and bisadducts of dirhodium(II) tetraacetate would so suggest.[21] The ΔH value for the loss of the first Me_2SO is approximately half that for the loss of the second Me_2SO, showing that the Rh–S(axial) bond in the monoadduct is considerably stronger than those in the bisadduct. Another interesting aspect of the $Rh_2(tcl)_4(tclH)$ structure is the S–Rh–Rh–N average torsional angle of 21.1°. An approximate

(17) Germain, G.; Main, P.; Woolfson, M. M. *Acta Crystallogr., Sect. A: Cryst. Phys., Diffr., Theor. Gen. Crystallogr.* **1971**, *A27*, 368.
(18) Bijvoet, J. M.; Peerdeman, A. F.; Van Bommel, A. J. *Nature (London)* **1951**, *168*, 271.
(19) Cotton, F. A.; Felthouse, T. R. *Inorg. Chem.* **1981**, *20*, 584.
(20) Norman, J. G.; Kolari, H. J. *J. Am. Chem. Soc.* **1978**, *100*, 791.
(21) Kitchens, J. F. Ph.D. Dissertation, The University of Houston, 1969.

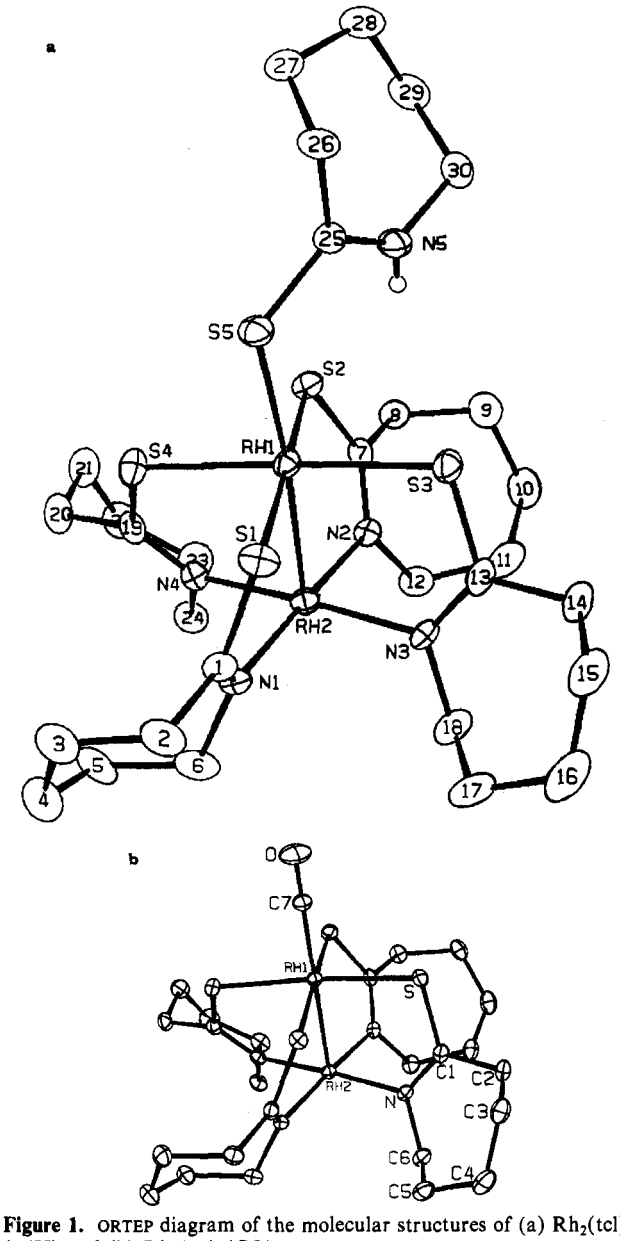

Figure 1. ORTEP diagram of the molecular structures of (a) $Rh_2(tcl)_4$(tclH) and (b) $Rh_2(tcl)_4$(CO).

20° torsional angle has also been observed for complexes with 6-methyl- and 6-chloro-2-oxypyridine anion bridges.[19] These complexes have three nitrogen donors bound to one rhodium. In these cases, the twist was attributed to repulsive forces due to the three adjacent 6-CH_3 or 6-Cl ring substituents. A model of $Rh_2(tcl)_4$(tclH) shows that increasing the S–Rh–Rh–N torsional angle results in greater distances between the methylene hydrogens around the axial site of Rh(2) (see Figure 1 for labeling) and is consistent with this suggestion.

Questions have been raised regarding the relationship between Rh–Rh bond distance and the bite angle of the bridging ion.[20] These questions can be addressed in relation to $Rh_2(tcl)_4$(tclH) since in this complex the ω-thiocaprolactam molecule is involved as both a bridging and a nonbridging ligand. The Rh–Rh distance in $Rh_2(tcl)_4$(tclH) is relatively large, and the S–Rh–Rh–N torsional angle is 21°, yet the S–C–N angle for the axial and bridging thiocaprolactams are almost the same (122.8° and (average) 121.4°, respectively). Thus, there appears to be no direct correlation between the bite angle of the bridging ligand and the Rh–Rh distance.

Another question to be addressed is why the 4,0 isomer forms when $Rh_2(O_2CCH_3)_4$ reacts with ω-thiocaprolactam whereas the 2,2 cis isomer forms when lactams and amides are used as the substituting ligands. Steric arguments have been used to explain

Table II. Positional Parameters and Their Estimated Standard Deviations[a]

atom	x	y	z	B, Å²
		(a) $Rh_2(tcl)_4$(tclH)		
Rh1	0.10334 (3)	0.16098 (2)	0.19191 (2)	2.43 (1)
Rh2	0.25585 (3)	0.21044 (2)	0.32083 (2)	2.51 (1)
S1	0.2010 (1)	0.19866 (6)	0.08171 (8)	3.54 (3)
S2	0.0083 (1)	0.12891 (6)	0.30900 (8)	3.19 (3)
S3	0.2219 (1)	0.07345 (6)	0.21477 (8)	3.37 (3)
S4	−0.0080 (1)	0.24999 (6)	0.17781 (8)	3.66 (4)
S5	−0.0378 (1)	0.12296 (6)	0.05626 (8)	3.45 (3)
N1	0.3005 (3)	0.2684 (2)	0.2272 (2)	0.69 (9)
N2	0.2174 (3)	0.1555 (2)	0.4204 (2)	2.55 (9)
N3	0.3817 (3)	0.1510 (2)	0.3064 (2)	2.8 (1)
N4	0.1390 (3)	0.2713 (2)	0.3451 (2)	2.9 (1)
N5	−0.0508 (3)	0.0213 (2)	0.1477 (2)	3.6 (1)
C1	0.2791 (4)	0.2605 (2)	0.1359 (3)	3.0 (1)
C2	0.3162 (4)	0.3044 (2)	0.0709 (3)	4.2 (1)
C3	0.2505 (5)	0.3642 (2)	0.0620 (3)	5.0 (2)
C4	0.2922 (5)	0.4065 (2)	0.1444 (4)	5.8 (2)
C5	0.2893 (5)	0.3815 (2)	0.2409 (3)	4.9 (1)
C6	0.3606 (4)	0.3250 (2)	0.2694 (3)	4.2 (1)
C7	0.1169 (4)	0.1287 (2)	0.4142 (3)	2.6 (1)
C8	0.0867 (4)	0.0966 (2)	0.4958 (3)	3.4 (1)
C9	0.1542 (5)	0.0380 (2)	0.5228 (3)	4.8 (1)
C10	0.2806 (5)	0.0464 (3)	0.5783 (3)	5.9 (2)
C11	0.3547 (5)	0.0857 (3)	0.5304 (3)	5.3 (2)
C12	0.3098 (4)	0.1498 (2)	0.5086 (3)	3.9 (1)
C13	0.3612 (4)	0.0966 (2)	0.2701 (3)	3.1 (1)
C14	0.4565 (4)	0.0517 (2)	0.2715 (3)	4.2 (1)
C15	0.5335 (5)	0.0687 (3)	0.2071 (4)	5.7 (2)
C16	0.6252 (4)	0.1163 (3)	0.2487 (3)	6.4 (2)
C17	0.5789 (4)	0.1756 (3)	0.2760 (3)	5.4 (2)
C18	0.5035 (4)	0.1704 (2)	0.3472 (3)	4.4 (1)
C19	0.0405 (4)	0.2855 (2)	0.2864 (3)	3.2 (1)
C20	−0.0433 (5)	0.3316 (2)	0.3097 (3)	4.5 (1)
C21	−0.0955 (4)	0.3091 (2)	0.3898 (4)	5.1 (1)
C22	−0.0158 (5)	0.3189 (2)	0.4874 (3)	5.0 (1)
C23	0.0996 (5)	0.2848 (2)	0.5059 (3)	4.3 (1)
C24	−0.1746 (4)	0.3011 (2)	0.4392 (3)	3.7 (1)
C25	−0.0860 (4)	0.0528 (2)	0.0687 (3)	2.8 (1)
C26	−0.1732 (4)	0.0247 (2)	−0.0121 (3)	3.6 (1)
C27	−0.2962 (4)	0.0154 (2)	0.0076 (3)	4.3 (1)
C28	−0.3003 (4)	−0.0409 (2)	0.0647 (3)	4.8 (1)
C29	−0.2173 (4)	−0.0428 (2)	0.1638 (3)	4.7 (1)
C30	−0.0891 (5)	0.0391 (2)	0.1652 (3)	4.3 (1)
		(b) $Rh_2(tcl)_4$(CO)		
Rh1	0.500	0.500	0.703	1.956 (8)
Rh2	0.500	0.500	0.48473 (8)	1.914 (8)
S	0.5911 (1)	0.6865 (1)	0.6937 (2)	2.59 (2)
O	0.500	0.500	0.9712	6.7 (2)
N	0.6368 (4)	0.6137 (4)	0.4784 (4)	2.24 (8)
C1	0.6647 (5)	0.6879 (5)	0.5618 (5)	2.5 (1)
C2	0.7619 (5)	0.7746 (5)	0.5500 (6)	3.1 (1)
C3	0.8825 (5)	0.7148 (6)	0.5524 (6)	3.9 (2)
C4	0.9175 (6)	0.6586 (6)	0.4364 (8)	4.4 (2)
C5	0.8335 (5)	0.5680 (6)	0.3909 (7)	3.6 (1)
C6	0.7091 (6)	0.6103 (6)	0.3707 (5)	3.1 (1)
C7	0.500	0.500	0.871 (1)	2.9 (1)

[a] Anisotropically refined atoms are given in the form of the isotropic equivalent thermal parameter defined as $^4/_3[a^2B_{11} + b^2B_{22} + c^2B_{33} + ab(\cos\gamma)B_{12} + ac(\cos\beta)B_{13} + bc(\cos\alpha)B_{23}]$.

the formation of polar $Rh_2(fhp)_4$ complex.[1] There is no question that the substitution of the first lactam bridge places some steric constraint at the axial site of the rhodium bound to the lactam nitrogen. However, the only steric difference in the lactam and thiolactam ligand is the difference in size of the sulfur and oxygen donor atoms. Of course, steric crowding would increase with each successive nitrogen bond to the same rhodium ion. Arguments may be made for kinetic and/or thermodynamic factors being involved in determining the molecular geometry since substituting ligands such as acetamide and thioacetic acid produces only the 2,2 cis arrangement.[13] With these ligands no steric effects are involved. There is no question that once the first ω-thiocaprolactamate bridge is formed, directing influences, probably both

Table III. Selected Bond Lengths (Å) and Bond Angles (deg)[a]

(a) $Rh_2(tcl)_4(tclH)$

Bond Lengths

Rh1–Rh2	2.497 (1)	N1–C1	1.299 (3)
Rh1–S1	2.346 (1)	N1–C6	1.489 (3)
Rh1–S2	2.367 (1)	N2–C7	1.306 (3)
Rh1–S3	2.359 (1)	N2–C12	1.462 (3)
Rh1–S4	2.343 (1)	N3–C13	1.310 (3)
Rh1–S5	2.388 (1)	N3–C18	1.470 (3)
Rh2–N1	2.032 (2)	N4–C19	1.293 (3)
Rh2–N2	2.025 (2)	N4–C24	1.480 (3)
Rh2–N3	2.029 (2)	N5–C25	1.316 (3)
Rh2–N4	2.016 (2)	N5–C30	1.451 (3)
S1–C1	1.723 (3)		
S2–C7	1.728 (3)		
S3–C13	1.712 (3)		
S4–C19	1.725 (3)		
S5–C25	1.677 (3)		

Bond Angles

Rh2–Rh1–S5	173.10 (2)	Rh1–S1–C1	105.4 (1)
Rh2–Rh1–S1	88.51 (2)	Rh1–S2–C7	105.0 (1)
Rh2–Rh1–S2	88.38 (2)	Rh1–S3–C13	106.5 (1)
Rh2–Rh1–S3	88.00 (2)	Rh1–S4–C19	104.6 (1)
Rh2–Rh1–S4	88.79 (2)	Rh1–S5–C25	114.8 (1)
Rh1–Rh2–N1	91.80 (7)	Rh2–N1–C1	125.7 (2)
Rh1–Rh2–N2	91.54 (7)	Rh2–N2–C7	125.7 (2)
Rh1–Rh2–N3	92.55 (7)	Rh2–N3–C13	124.7 (2)
Rh1–Rh2–N4	91.73 (7)	Rh2–N4–C19	125.7 (2)

(b) $Rh_2(tcl)_4(CO)$

Bond Lengths

Rh1–Rh2	2.495 (1)	C1–C2	1.493 (4)
Rh1–S	2.373 (1)	C2–C3	1.537 (5)
Rh2–N	2.033 (3)	C3–C4	1.524 (6)
Rh1–C7	1.913 (7)	C4–C5	1.503 (5)
C7–O	1.147 (8)	C5–C6	1.518 (5)
C1–S	1.724 (4)		
C1–N	1.314 (4)		

Bond Angles

Rh2–Rh1–C7	180.00 (0)	S–Rh1–C7	92.57 (3)
Rh2–Rh1–S	87.43 (3)	S–C1–N	120.6 (2)
Rh2–N–C1	125.0 (2)	S–C1–C2	116.6 (3)
Rh2–N–C6	116.1 (2)	C1–N–C6	118.9 (3)
Rh1–C7–O	180.00 (0)	C1–C2–C3	111.7 (3)
Rh1–Rh2–N	91.93 (9)	C2–C3–C4	114.0 (3)
Rh1–S–C1	105.1 (1)	C3–C4–C5	114.9 (3)
N–C1–C2	122.8 (3)	C4–C5–C6	115.5 (4)
N–C6–C5	113.8 (3)		

[a] Numbers in parentheses are estimated standard deviations in the least significant digits.

steric and electronic, are set in motion that influence each successive ligand substitution.

The bond distances and angles of the "cage unit" of $Rh_2(tcl)_4(CO)$ are remarkably similar to those of $Rh_2(tcl)_4(tclH)$ (see Tables II and III and Figure 1). The Rh–Rh bond distances are essentially the same for the two complexes. This is unexpected since the electronic absorption spectra and the electrochemistry (see following section) of the two complexes are quite different. This may mean that the Rh–Rh distance in this highly polar complex is not as sensitive to axial perturbations as are other dirhodium(II) complexes.

The Rh–C distance of 1.913 Å for the rhodium–carbonyl bond falls within the range of distances for other rhodium complexes with terminal carbonyls. This work presents the first structure of a CO monoadduct of a dirhodium(II) complex, and therefore structural comparisons to other similar systems are not possible. Christoph and Koh reported[22] the low-temperature (−104 °C) crystal structure of $Rh_2(O_2CCH_3)_4(CO)_2$. They found a 2.092-Å Rh–CO bond distance, which is longer by 0.179 Å than the 1.913 Å for $Rh_2(tcl)_4(CO)$. There is no question that the Rh–CO interaction in the latter complex is much stronger. This is most probably due to a large π component in the rhodium–carbonyl bond.[23]

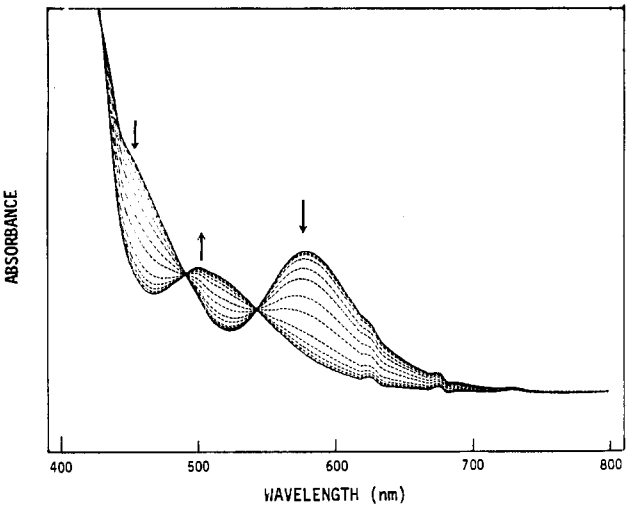

Figure 2. Time-resolved electronic absorption spectra recorded during the reaction of CO with $Rh_2(tcl)_4(tclH)$ in $C_2H_4Cl_2$.

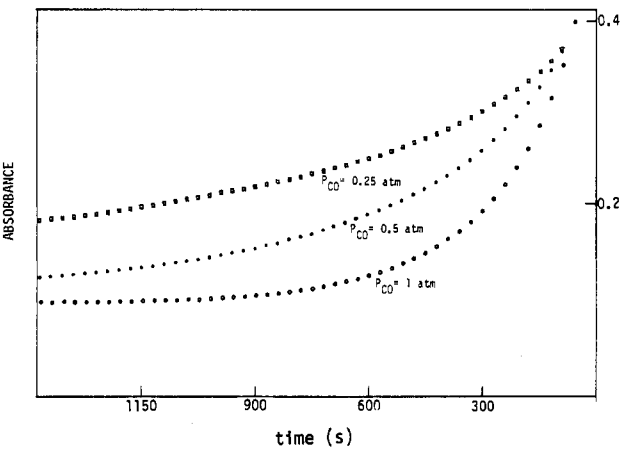

Figure 3. Change of absorbance at λ = 578 nm during the reaction of $Rh_2(tcl)_4(tclH)$ with different partial pressures of CO.

Axial Ligand Exchange of $Rh_2(tcl)_4(tclH)$. The axial ligand exchange reactions of dirhodium(II) carboxylates, amidates, lactamates, and amidinates are rapid and reversible.[8,9,12,14] The bound axial tclH ligand in $Rh_2(tcl)_4(tclH)$ does not appear to undergo substitution by ligands such as pyridine, CH_3CN, cyanopyridine, *N*-methylimidazole, and phosphines. This is true even after hours of exposure to these ligands. However, when a solution of $Rh_2(tcl)_4(tclH)$ is exposed to carbon monoxide in CH_2Cl_2 or 1,2-dichloroethane ($C_2H_4Cl_2$), a unidirectional exchange occurs. This reaction can be followed by the time-resolved electronic absorption spectra shown in Figure 2.

$Rh_2(tcl)_4(tclH)$ has a peak in the electronic absorption spectrum at 578 nm ($\epsilon = 3.2 \times 10^2$ M^{-1} cm^{-1}) and a shoulder at ~455 nm. Upon exposure to CO both of these peaks disappear and a new peak appears at ~500 nm ($\epsilon = 3.0 \times 10^2$ M^{-1} cm^{-1}). A well-defined set of isosbestic points are observed (λ = 543, 491, 430 nm) during this change, indicating the presence of only two detectable dirhodium species in solution.

The kinetics of the reaction of $Rh_2(tcl)_4(tclH)$ with CO was studied by monitoring changes in the absorbance at different wavelengths under a constant CO pressure. Figure 3 shows the loss of absorbance at 580 nm for a 3.1×10^{-3} M solution of $Rh_2(tcl)_4(tclH)$ exposed to constant CO pressures of 1, 0.5, and 0.25 atm. At all pressures, the first half-life is inversely pro-

(22) Christoph, G. G.; Koh, Y.-B. *J. Am. Chem. Soc.* **1979**, *101*, 1422.

(23) Chavan, M. Y.; Ahsan, M. Q.; Lifsey, R. S.; Bear, J. L.; Kadish, K. M. *Inorg. Chem.* **1986**, *25*, 3218.

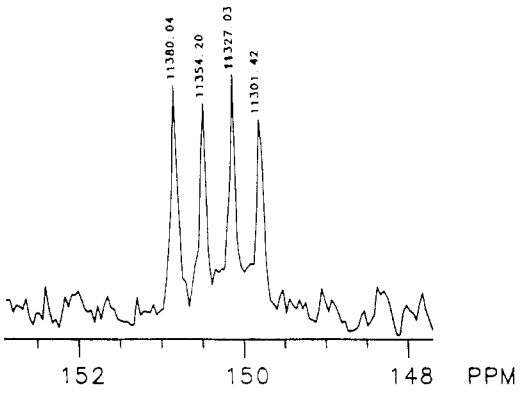

Figure 4. Portion of the ^{13}C NMR spectrum of $Rh_2(tcl)_4(CO)$ showing the rhodium–carbon coupling. J_{Rh1-C} = 52.90 Hz; J_{Rh2-C} = 25.73 Hz. Chemical shifts are labeled in Hz.

portional to P_{CO}. Calculated values of the first half-life were ~300 s at 1 atm of CO, ~600 s at 0.5 atm of CO, and ~1150 s at 0.25 atm of CO. The first half-life was independent of the $Rh_2(tcl)_4(tclH)$ concentration at a given CO partial pressure. Solutions containing different concentrations of $Rh_2(tcl)_4(tclH)$ (3.1×10^{-3}, 1.55×10^{-3}, 0.8×10^{-3} M) were exposed to a constant pressure of 1 atm of CO, but the first half-life remained invariant at ~300 s.

These data fit the rate law given by eq 1, where Rh_2L = $Rh_2(tcl)_4(tclH)$.

$$-d[Rh_2L]/dt = k[CO][Rh_2L] \quad (1)$$

Equation 1 can be rewritten in terms of P_{CO} with use of Henry's law constant (k_H):

$$-d[Rh_2L]/dt = kk_HP_{CO}[Rh_2L] \quad (2)$$

The values of P_{CO} were kept constant throughout a given experiment. Assuming [CO] is constant under these conditions, eq 2 becomes

$$-d[Rh_2L]/dt = k'P_{CO}[Rh_2L] \quad (3)$$

where $k' = kk_H$ and

$$-d[Rh_2L]/dt = k''[Rh_2L] \quad (4)$$

where $k'' = k'P_{CO} = kk_HP_{CO}$. Plots of ln $[Rh_2L]$ vs. time at P_{CO}'s of 1, 0.5, and 0.25 atm respectively give $k'' = k'P_{CO} = 2.6 \times 10^{-3}$, 1.6×10^{-3}, and 1.0×10^{-3} s^{-1}. From these k'' values, k' values of 2.4×10^{-3}, 3.2×10^{-3}, and 4.0×10^{-3} s^{-1} atm^{-1} are obtained.

Since eq 4 is pseudo first order, $t_{1/2} = (\ln 2)/k'' = (\ln 2)/k'P_{CO}$. A linear plot of $t_{1/2}$ vs. $1/P_{CO}$ gives a slope of $(\ln 2)/k'$. The k' value obtained in this manner is 2.3×10^{-3} s^{-1} atm^{-1}. The k' values obtained by two different methods appear to be reasonably consistent, indicating that the data obey eq 1 and that the reaction is first order in both $Rh_2(tcl)_4(tclH)$ and CO. No measurable rate dependence on [tclH] was observed.

The kinetic study of the reaction of CO with $Rh_2(tcl)_4(tclH)$ suggests that only the CO monoadduct is formed as the final product. The molecular structure of the product was determined to establish the nature of the CO adduct and to evaluate the effect of CO bonding to the dirhodium(II) unit. The results show that the axial tclH ligand is lost in this reaction and that $Rh_2(tcl)_4(CO)$ is the isolated product.

The fact that the CO monoadduct is isolated as the only product in the solid state does not rule out the possibility of a CO bisadduct existing in solution. For this reason the ^{13}C NMR spectrum of a $Rh_2(tcl)_4$ solution saturated with ^{13}CO was obtained. The ^{13}C NMR spectrum of $Rh_2(tcl)_4(^{13}CO)$ (Figure 4) shows a doublet of doublets in the carbonyl region. The peaks occur at 150.81, 150.47, 150.11, and 149.77 ppm referenced to $CDCl_3$. This AMX pattern is consistent with one axially bound ^{13}CO split into a doublet of doublets by two nonequivalent Rh atoms ($I = {}^1/_2$). The coupling constants are J_{Rh1-C} = 52.89 Hz and J_{Rh2-C} = 25.72 Hz for the bound and unbound Rh atoms, respectively. It should be noted that the chemical shift centered at 150.29 ppm is farther upfield than any previously reported rhodium–carbonyl species.[24]

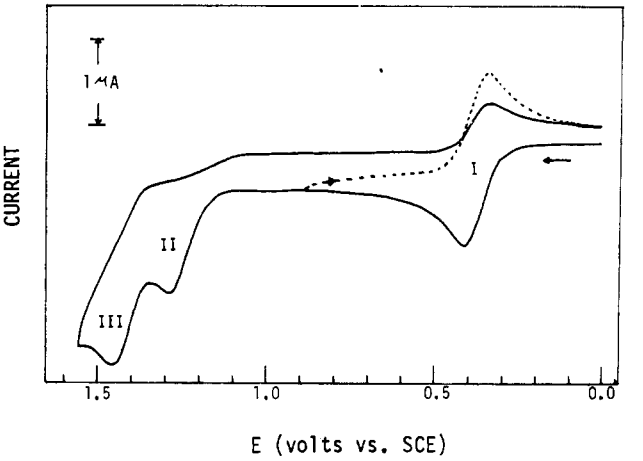

Figure 5. Cyclic voltammogram of 1 mM $Rh_2(tcl)_4(tclH)$ in $C_2H_4Cl_2$ containing 0.1 M TBAP under nitrogen (scan rate 100 mV/s).

The kinetic data suggest that substitution of the axial tclH ligand by CO is first order in both $Rh_2(tcl)_4(tclH)$ and CO. Also, $Rh_2(tcl)_4(tclH)$ is relatively inert to substitution by other ligands. Even concentrated solutions of pyridine, cyanopyridine, *N*-methylimidazole, and triphenylphosphine do not substitute for tclH at any detectable rate. Therefore, it appears unlikely that tclH substitution is initiated by a prior dissociative step. However, the data strongly support an associative mechanism for the exchange process, which could occur by two possible pathways. One conceivable pathway is that CO first binds to the vacant axial site of the rhodium having four Rh–N bonds (Rh2 in Figure 1). This could labilize the tclH at the other axial site, resulting in rapid dissociation of the tclH ligand. The second CO then binds to the vacated site followed by dissociation of the initial CO molecule. The rate-limiting step in this process is the formation of the first CO bond to the sterically crowded axial site of Rh2. This mechanism also explains why more bulky ligands do not initiate the exchange process. The other pathway involves attachment of the incoming CO to Rh1, thus forming a transient seven-coordinate rhodium center from which the tclH then dissociates. The fact that Rh1 is bound to four large sulfur donors and that the two π^* metal-centered molecular orbitals are filled argues against an associative step involving Rh1.

Electrochemistry of $Rh_2(tcl)_4(tclH)$. The strong electron-donating nature of amidate bridging ligands results in a stepwise negative shift of the first oxidation potential[7-9] as *n* varies from 4 to 0 in $Rh_2(O_2CCH_3)_n(HNOCCH_3)_{4-n}$. This electrode reaction is shown by reaction 5.

$$Rh^{II}Rh^{II} \rightleftharpoons Rh^{II}Rh^{III} + e^- \quad (5)$$

The electrochemical and geometrical properties of dirhodium complexes with mixed donor atom ligands are quite different from those of the carboxylates. Dirhodium complexes with mixed donor ligands undergo two reversible one-electron oxidations to form $Rh^{II}Rh^{III}$ (reaction 5) and $Rh^{III}Rh^{III}$. In contrast, dirhodium carboxylates only undergo a single electrooxidation process within the solvent range. Only a single dirhodium complex has been reported to be reversibly reduced to form a $Rh^{II}Rh^{I}$ species.[11]

The cyclic voltammogram of $Rh_2(tcl)_4(tclH)$ in $C_2H_4Cl_2$ containing 0.1 M TBAP is shown in Figure 5. No reductions of $Rh_2(tcl)_4(tclH)$ were observed up to −1.6 V in CH_2Cl_2 or CH_3CN. A reversible one-electron oxidation (process I) is observed at $E_{1/2}$ = 0.37 V vs. SCE. Two additional irreversible oxidation peaks (processes II and III) are observed at E_p = 1.28 and 1.45 V, when the scan rate is 0.1 V/s.

A similar cyclic voltammogram is obtained in CH_3CN. The first oxidation is quasi-reversible in this solvent (ΔE_p = 80 mV

(24) *^{13}C NMR Data for Organometallic Compounds*; Mann, B. E., Taylor, B. F., Eds.; Academic: New York, 1981; pp 178–179.

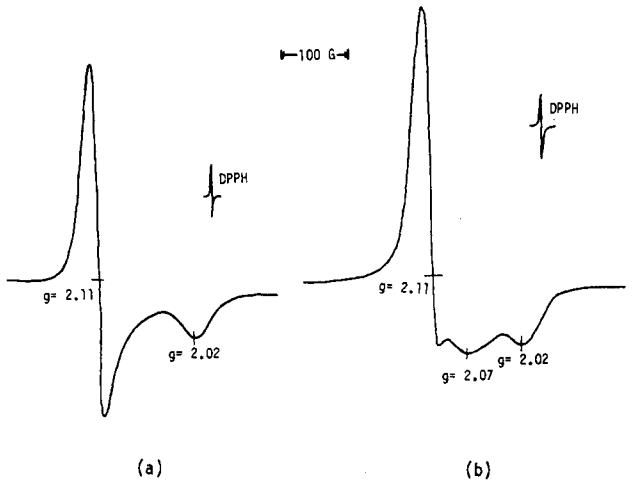

Figure 6. Low-temperature ESR spectra of the products of the one-electron oxidation of $Rh_2(tcl)_4(tcl)$ in (a) CH_3CN and (b) $C_2H_4Cl_2$, both containing 0.1 M TBAP.

at 0.1 V/s) and occurs at $E_{1/2} = 0.34$ V. Also, two ill-defined irreversible oxidations occur at $E_p = \sim 1.3$ and ~ 1.5 V. Reversing the scan at 1.6 V results in no rereduction for processes II and III (see Figure 5). Also, the cathodic peak of process I is higher if one does not scan to potentials positive of the two additional oxidation peaks (see dashed line, Figure 5).

Increasing the sweep rate does not improve the reversibility of processes II and III. As the sweep rate increases from 0.1 V/s, the peak potential of process II shifts to more positive values while that of process III remains relatively unchanged. In fact, at 5 V/s peaks II and III have merged to give one irreversible peak in which the two processes are overlapped.

Free ω-thiocaprolactam is oxidized at $E_p = 1.15$ V in $C_2H_4Cl_2$ containing 0.1 M TBAP, and it is possible that process II is the oxidation of free ω-thiocaprolactam that dissociates as a result of the first oxidation step (process I). Thus, if bound and unbound tclH are in equilibrium, we would expect to see a positive shift in E_p as the scan rate increases. In this case, process III would be due to an oxidation of either the $[Rh_2(tcl)_4]^+$ complex or an equatorial ligand of this complex. However, because of the uncertainties in processes II and III and their irreversibility, we have only characterized the oxidation associated with process I.

Solutions of $Rh_2(tcl)_4(tclH)$ were bulk-electrolyzed in CH_3CN and $C_2H_4Cl_2$ at 0.6 V under a nitrogen atmosphere, after which the ESR spectra of the singly oxidized species were recorded. No ESR signal was observed at room temperature, but low-temperature spectra were obtained. Figure 6a shows an ESR spectrum of singly oxidized $Rh_2(tcl)_4(tclH)$ at <−150 °C in CH_3CN. This axial ESR spectrum has $g_\perp = 2.11$ and $g_\parallel = 2.02$ and is similar in shape to that of $[Rh_2(O_2CR)_n(RNOCR')_{4-n}]^+$ complexes.[4,6] However, there are two important differences in these spectra. The first is that for the spectrum in Figure 6a $g_\parallel$ is greater than g_e while $[Rh_2(O_2CCH_3)_n(RNOCR')_{4-n}]^+$ has a $g_\parallel$ value that is always observed to be less than g_e.[6,8] Furthermore, the $g_\parallel$ signal in Figure 6a shows no resolution of the hyperfine splitting due to the two rhodium nuclei (^{103}Rh, $I = {}^1/_2$). This is in contrast[6,8] to the 1:2:1 triplets observed for $[Rh_2(O_2CCH_3)_n(RNOCR')_{4-n}]^+$.

The ESR spectrum obtained after the one-electron oxidation of $Rh_2(tcl)_4(tclH)$ in $C_2H_4Cl_2$ (Figure 6b) is somewhat different from that in CH_3CN. In this solvent there are two signals at $g = 2.11$ ($g_\perp$) and $g = 2.02$ ($g_\parallel$) and a third signal at $g = 2.07$. None of the signals show a resolved hyperfine structure. The axial environment of $Rh^{II}Rh^{III}$ is not clear from the ESR spectrum, but the type of axial binding in CH_3CN does not appear to be the same as that in $C_2H_4Cl_2$. The axial tclH ligand seems to be lost upon bulk electrolysis in CH_3CN, but this ligand may be at least partly retained in $C_2H_4Cl_2$. This would result in a complicated ESR spectrum composed of two overlapping signals. The spectrum in Figure 6a is assigned to $[Rh_2(tcl)_4]^+$, and the signal in Figure 6b is assigned to a mixture of $[Rh_2(tcl)_4]^+$ and $[Rh_2(tcl)_4(tclH)]^+$.

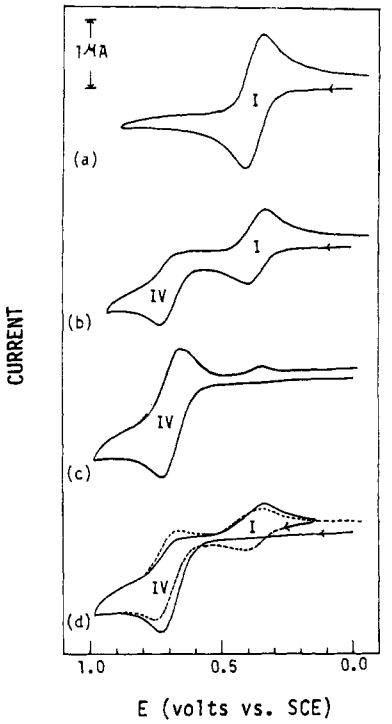

Figure 7. Cyclic voltammograms of 1 mM $Rh_2(tcl)_4(tclH)$ in $C_2H_4Cl_2$ containing 0.1 M TBAP (scan rate 100 mV/s): (a) under nitrogen; (b) after 10-min exposure to 0.4 atm of CO; (c) after 10-min exposure to 1 atm of CO; (d) upon removal of free CO from the above solution by bubbling N_2.

These assignments are supported by electrochemical and ESR data presented in a later section.

The first oxidation of $Rh_2(tcl)(tclH)$ in $C_2H_4Cl_2$ can be expressed by eq 6.

$$Rh_2(tcl)_4(tclH) \rightleftarrows [Rh_2(tcl)_4(tclH)]^+ + e^- \quad (6)$$

The $[Rh_2(tcl)_4(tclH)]^+$ formed by reaction 6 may be in equilibrium with axially unligated $[Rh_2(tcl)_4]^+$ such as shown by eq 7.

$$[Rh_2(tcl)_4(tclH)]^+ \rightleftarrows [Rh_2(tcl)_4]^+ + tclH \quad (7)$$

A possible dissociation of tclH from $[Rh_2(tcl)_4(tclH)]^+$ has been discussed in terms of the oxidation peaks II and III in the cyclic voltammograms. In addition, the ESR spectroscopic data also suggest the presence of reaction 7 on a bulk electrolysis time scale.

Electrochemistry of $Rh_2(tcl)_4(tclH)$ under a CO Atmosphere. Figure 7 shows cyclic voltammograms of 1 mM $Rh_2(tcl)_4(tclH)$ in $C_2H_4Cl_2$ exposed to different partial pressures of CO. A reversible oxidation wave (process I) is observed at $E_{1/2} = 0.37$ V under a nitrogen atmosphere (Figure 7a). After exposure to 0.4 atm of CO a new oxidation wave that appears to be irreversible is observed at more positive potentials (Figure 7b). This new wave appears at $E_p = 0.74$ V (process IV) and is assigned as due to the oxidation of $Rh_2(tcl)_4(CO)$.

It is noteworthy that currents for the $Rh_2(tcl)_4(tclH)$ oxidation (process I) diminish in magnitude upon exposure to CO but at the same time the oxidation potential of process I is insensitive to the partial pressure of CO. Clearly, $Rh_2(tcl)_4(tclH)$ and $Rh_2(tcl)_4(CO)$ are not in equilibrium. This is also suggested by the electronic absorption spectra, which were discussed in a previous section.

Solutions of $Rh_2(tcl)_4(tclH)$ exposed to 1 atm of CO for 10 min give the cyclic voltammogram shown in Figure 7c. Process I has almost completely disappeared under these conditions, and there is a single oxidation process at $E_{1/2} = 0.71$ V. A reaction at this same potential was earlier assigned to the $[Rh_2(tcl)_4(CO)]^{0/+}$ couple. The peak to peak separation (ΔE_p) of 60 mV suggests a reversible one-electron transfer under 1 atm of CO. However, the ratio of the cathodic peak current to the anodic peak current

Scheme I

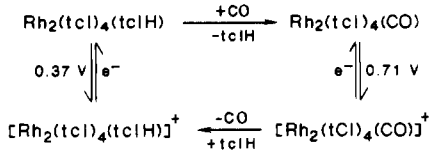

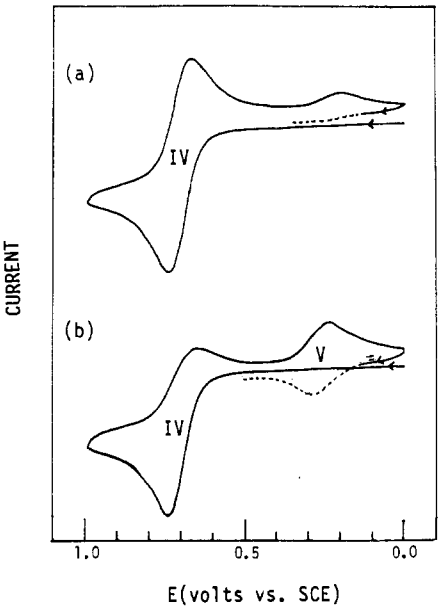

Figure 8. Cyclic voltammograms of 1 mM $Rh_2(tcl)_4(CO)$ in $C_2H_4Cl_2$ containing 0.1 M TBAP (scan rate 100 mV/s): (a) under 1 atm of CO; (b) under N_2 atmosphere.

(i_{pc}/i_{pa}) is ~0.8 at 0.1 V/s, thus suggesting the occurrence of a chemical reaction following oxidation of $Rh_2(tcl)_4(CO)$. In addition, another small cathodic peak is observed at $E_{pc} = 0.34$ V if the scan is reversed at potentials positive of 0.8 V.

The cyclic voltammogram illustrated in Figure 7d was obtained when nitrogen was bubbled through solutions of $Rh_2(tcl)_4(CO)$ that also contained equimolar concentrations of displaced tclH. As seen in this figure, there is still an oxidation peak of 0.74 V, suggesting that the axial CO ligand of $Rh_2(tcl)_4(CO)$ is not rapidly lost. Figure 7d differs from Figure 7c in that the oxidation of $Rh_2(tcl)_4(CO)$ shows characteristics of a reversible electron transfer followed by an irreversible chemical reaction; i.e., $|E_{pa} - E_{p/2}| = 60$ mV and $i_{pc}/i_{pa} << 1$. When the scan rate was increased to 10 V/s, the i_{pc}/i_{pa} ratio approached 1.0.

Reversal of the scan at potentials more positive than 0.8 V and at a scan rate of 0.1 V/s showed a cathodic peak at 0.34 V. This peak was coupled to an oxidation peak at ~0.41 V and suggests that this "new" electrode reaction is the same one as that shown by process I in Figure 7. The data also suggest that oxidation of $Rh_2(tcl)_4(CO)$ in the presence of tclH generates $[Rh_2(tcl)_4(CO)]^+$, which, in the absence of a CO atmosphere, is rapidly converted to $[Rh_2(tcl)_4(tclH)]^+$. These observations are summarized by the overall oxidation/reduction pathways shown in Scheme I.

Electrochemistry of $Rh_2(tcl)_4(CO)$ in the Absence of Free tclH. Figure 8 illustrates the cyclic voltammograms of $Rh_2(tcl)_4(CO)$ in $C_2H_4Cl_2$ under 1 atm of CO and under pure nitrogen. $Rh_2(tcl)_4(CO)$ is reversibly oxidized at $E_{1/2} = 0.71$ V under 1 atm of CO (Figure 8a). However, in the absence of CO (Figure 8b) the oxidation becomes less reversible and the reverse (negative) scan shows a new peak at 0.22 V. This reduction peak is coupled to an anodic oxidation peak at 0.28 V, which is not present in the initial positive scan.

Controlled-potential oxidation of $Rh_2(tcl)_4(CO)$ was carried out at 0.9 V under N_2 and resulted in the total disappearance of the $[Rh_2(tcl)_4(CO)]^{0/+}$ couple. After bulk oxidation, only the reaction at $E_{1/2} = 0.25$ V (process V) was observed. This oxidation/reduction is attributed to $[Rh_2(tcl)_4]^{0/+}$. No significant changes were observed in the UV–visible spectrum when pure CO was bubbled through this oxidized solution at room temperature. Also, no changes were observed in the low-temperature ESR spectrum (discussed below) under CO.

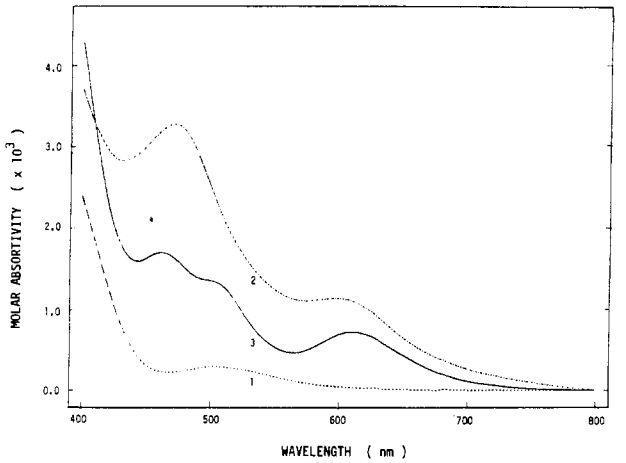

Figure 9. Visible spectra of (1) $Rh_2(tcl)_4(CO)$, (2) $[Rh(tcl)_4]^+$ generated by electrooxidation of $Rh_2(tcl)_4(CO)$, and (3) $Rh_2(tcl)_4$ generated by electrochemical reduction of $[Rh_2(tcl)_4]^+$ (solvent $C_2H_4Cl_2$ containing 0.1 M TBAP).

Controlled-potential oxidation of $Rh_2(tcl)_4(CO)$ under nitrogen generates $[Rh_2(tcl)_4]^+$, which can be reversibly reduced[25] at $E_{1/2} = 0.25$ V to give $Rh_2(tcl)_4$. The overall oxidation of $Rh_2(tcl)_4(CO)$ can be given by eq 8–10. The visible spectra of $Rh_2(tcl)_4(CO)$,

$$Rh_2(tcl)_4(CO) \rightleftarrows [Rh_2(tcl)_4(CO)]^+ + e^- \qquad E_{1/2} = 0.71 \text{ V} \tag{8}$$

$$[Rh_2(tcl)_4(CO)]^+ \rightarrow [Rh_2(tcl)_4]^+ + CO \tag{9}$$

$$[Rh_2(tcl)_4]^+ + e^- \rightleftarrows Rh_2(tcl)_4 \qquad E_{1/2} = 0.25 \text{ V} \tag{10}$$

$[Rh_2(tcl)_4]^+$, and $Rh_2(tcl)_4$ are shown in Figure 9. $Rh_2(tcl)_4(CO)$ has a peak at 500 nm ($\epsilon = 3 \times 10^2$ M^{-1} cm^{-1}; Figures 2 and 9). Upon oxidation under nitrogen, $[Rh_2(tcl)_4]^+$ is formed on a coulometric time scale. The spectrum of $[Rh_2(tcl)_4]^+$ has an intense absorbance peak at 480 nm ($\epsilon = 3.3 \times 10^3$ M^{-1} cm^{-1}) and another less intense peak at 600 mm ($\epsilon = 1.4 \times 10^3$ M^{-1} cm^{-1}). $Rh_2(tcl)_4$ is formed by reduction of $[Rh_2(tcl)_4]^+$ and has three peaks at 465, ~500, and 610 nm ($\epsilon = 8 \times 10^2$ M^{-1} cm^{-1}).

ESR Spectrum of Electrochemically Generated $[Rh_2(tcl)_4]^+$. $[Rh_2(tcl)_4]^+$ was generated by controlled-potential oxidation of $Rh_2(tcl)_4(CO)$ in $C_2H_4Cl_2$ under a nitrogen atmosphere. Its low-temperature ESR spectrum has $g_\perp = 2.09$ and $g_\parallel \simeq 2.02$ and is nearly identical with the ESR spectrum obtained after the one-electron oxidation of $[Rh_2(tcl)_4(tclH)]^+$ in CH_3CN (Figure 6a). The similarities in the two ESR spectra further support the suggestion that bulk oxidation of $Rh_2(tcl)_4(tclH)$ in CH_3CN leads to total loss of the tclH axial ligand but a similar oxidation in $C_2H_4Cl_2$ results in partial retention of the tclH axial ligand.

Summary and Conclusions. Our results are of interest for other dirhodium(II) complexes and for metal–metal bonds in general. The structure of the $Rh_2(tcl)_4$ unit shows that the two rhodiums have different equatorial bonds (see Figure 1) and ought to be electronically nonequivalent. This is true regardless of the axial ligands. The two rhodium atoms in $[Rh_2((PhN)_2CPh)_4]^+$ have identical equatorial environments, but in CH_3CN they are unequivalent by ESR. Consequently, it was suggested that CH_3CN

(25) The oxidation of $Rh_2(tcl)_4(CO)$ under a nitrogen atmosphere also produces a small amount of a species that is irreversibly reduced at about −0.2 V. The overall cycle

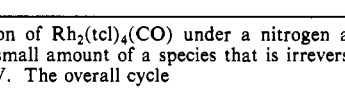

is not totally quantitative.

was bound at only one of the two axial sites.[11] For this complex, the $g_\parallel$ was observed to be split into a doublet of doublets instead of the 1:2:1 triplet invariably observed for dirhodium complexes where the two centers are equivalent.[6,8,11] Unfortunately, $[Rh_2(tcl)_4]^+$ does not show resolved hyperfine splitting, and the distribution of unpaired electron spin density on the two metal centers (see Figure 6a) remains unknown.

Half-wave potentials for oxidation of the three complexes discussed in this paper increase in the order $Rh_2(tcl)_4 < Rh_2(tcl)_4(tclH) < Rh_2(tcl)_4(CO)$. This indicates a lowering of the HOMO upon tclH or CO binding. Lowering of the HOMO upon axial binding by π acceptors is also observed for $Rh_2(O_2CCH_3)_n(HNOCCH_3)_{4-n}$.[23] This is in contrast to the dirhodium carboxylates in that the HOMO is raised in energy upon axial binding to a π-acid ligand.[8] As a consequence, it was suggested that the HOMO of the dirhodium acetamidate complexes was a π^* orbital.[8,12,23] However, theoretical calculations predict an ESR spectrum in which $g_\parallel >> g_e$[26] for a π^* HOMO. The fact that the ESR spectra of $[Rh_2(O_2CCH_3)_n(RNOCR')_{4-n}]^+$ complexes always have $g_\parallel \ll g_e$ contradicts a π^* HOMO. In the case of $[Rh_2(tcl)_4]^+$, $g_\parallel$ is greater than g_e but $g_\perp$ is greater still. On the basis of theoretical predictions[26] involving dirhodium carboxylates, the HOMO of $[Rh_2(tcl)_4]^+$ should therefore have σ symmetry.

In the last few years numerous axial ESR spectra ($g_\perp > g_\parallel$) of singly oxidized dirhodium(II,III) complexes have been reported in which $g_\parallel << g_e$,[6,8] $g_\parallel = g_e$,[11] and $g_\parallel > g_e$ (this work). *However, the effect of π-acceptor axial ligands on oxidation potentials of dirhodium(II,II) complexes (amidates, amidinates) is qualitatively the same in all cases.* The lowering of the HOMO due to the binding of only one CO by $Rh_2(tcl)_4$ is extremely large (0.45 V) while for $Rh_2(HNOCCH_3)_4$ axial binding by a single CO results in a smaller lowering of the HOMO ($\sim$0.3 V).[23] It is doubtful that the HOMO for these complexes is a δ^* orbital since the energy of this orbital should be relatively insensitive to axial bonding. However, the HOMO does not have to be the same for the neutral complex and the radical cation. One other point should be made. The substitution of bridging carboxylates by strongly basic ligands such as amidates raises the energy of the metal-centered d orbital MO's by approximately 1 V.[8] Since the 5s and 5p orbitals are less shielded, they should become closer in energy to the 4d orbitals. This would result in greater mixing of these orbitals into the Rh–Rh and Rh–L bonding scheme. For this reason theoretical calculations based on dirhodium carboxylates where little mixing is involved may not be applicable in this case.

(26) Kawamura, T.; Fukamachi, K.; Hayashida, S.; Yonezawa, T. *J. Am. Chem. Soc.* **1981**, *103*, 364.

This increased CO-binding ability of $Rh_2(tcl)_4$ over that of $Rh_2(HNOCCH_3)_4$ is consistent with a correlation proposed earlier.[23] It was observed that the magnitude of the CO binding constants for $Rh_2(O_2CCH_3)_n(HNOCCH_3)_{4-n}$ were related to $E_{1/2}$ for the oxidation of $Rh^{II}Rh^{II}$ to $Rh^{II}Rh^{III}$. More negative half-wave potentials correlate with higher CO binding constants. The half-wave potential for the $[Rh_2(tcl)_4]^{0/+}$ couple in $C_2H_4Cl_2$ (reaction 10) is $\sim$80 mV more negative than the $E_{1/2}$ value estimated[23] for the $[Rh_2(HNOCCH_3)_4]^{0/+}$ reaction in $C_2H_4Cl_2$ (0.25 V). If the same relationship holds, the K_{CO} value for $Rh_2(HNOCCH_3)_4$ is calculated to be $\sim 5 \times 10^3$ atm^{-1} while that for $Rh_2(tcl)_4$ would be 1.8×10^4 atm^{-1}.

The kinetic inertness of the Rh–L axial bond in $Rh_2(tcl)_4(tclH)$ is unusual for a dirhodium(II) complex. Rapid axial ligand exchange has been observed for all other bridged complexes whether bridged by homo or hetero donor atoms. The bimolecular nature of the substitution of CO for axial-bound tclH also raises some interesting mechanistic questions. It is hard to rationalize a seven-coordinate rhodium transition state since the π^* orbitals are filled and would interfere with an approaching ligand. A mechanism involving the formation of a kinetically labile transient bisadduct seems more attractive. The cavity at the axial site of Rh2 is small because of the inward projection of the CH_2 hydrogens. Therefore, only small ligands such as CO can interact with Rh2 and initiate the axial ligand exchange on Rh1. A slow axial ligand exchange is observed for $Rh_2(tcl)_4CO$ in the absence of CO pressure. Also, the oxidation of $Rh_2(tcl)_4L$ in bonding and nonbonding solvents results in rapid dissociation of L. This suggests that the HOMO of $Rh_2(tcl)_4L$ is a Rh–L π-bonding molecular orbital resulting from the filled Rh–Rh π^* orbital and empty orbitals of π symmetry on L. The fact that the $E_{1/2}$ value for oxidation of $Rh_2(tcl)_4CO$ is 0.45 V more positive than for oxidation of $Rh_2(tcl)_4$ supports this argument.

Acknowledgment. The support of the Robert A. Welch Foundation (K.M.K., Grant E-680; J.L.B., Grant E-918) is gratefully acknowledged. X-ray analysis was performed at the University of Houston X-ray Crystallography Center by Dr. James Korp.

Registry No. **1**, 106434-44-0; **2**, 106420-46-6; $[Rh_2(tcl)_4(tclH)]^+$, 106434-45-1; $[Rh_2(tcl)_4]^+$, 106420-47-7; $[Rh_2(tcl)_4(CO)]^+$, 106420-48-8; $Rh_2(O_2CCH_3)_4$, 15956-28-2; CO, 630-08-0.

Supplementary Material Available: Listings of derived atomic positional parameters, anisotropic thermal parameters, and root-mean-square amplitudes of thermal vibration and views of the unit cell for $Rh_2(tcl)_4(CO)$ and $Rh_2(tcl)_4(tclH)$ and a complete listing of bond distances and angles for $Rh_2(tcl)_4(tclH)$ (14 pages); listings of observed and calculated structure factors for both complexes (16 pages). Ordering information is given on any current masthead page.